# UNIGNITED HIGH-PRESSURE METHANE JET IMPINGING A PIPE RACK: PRACTICAL TOOLS FOR RISK ASSESSMENT

Cristian Colombini, Giuliana Maugeri, Gianluca Zanon, Renato Rota, Valentina Busini*

*Politecnico di Milano - Department of Chemistry, Materials and Chemical Engineering "Giulio Natta", Piazza Leonardo da Vinci 32, 20133, Milano, Italy*

* Corresponding author:

*E-mail address: valentina.busini@polimi.it*

## ABSTRACT

Although the diffusion of its storage and transport under liquefied conditions, nowadays it is common to have methane in gaseous form in several industrial applications. This leads to safety implications to be considered: hazards are linked to both the high-pressure at which the gas is kept and to its flammability. Scenarios where flammable jets impact an obstacle are of paramount importance because of their possible occurrence. Following a numerical approach, literature shows up that their assessment can be reliably performed by means of only Computational Fluid Dynamics tools. However, despite the improvements of computing power, Computational Fluid Dynamics costs still limit its use in daily risk analysts' activities. Therefore, considering an accidental jet-obstacle scenario of industrial interest, the present work investigates how a pipe rack can influence the development of a high-pressure methane jet. Based on a Computational Fluid Dynamics analysis, main achievements of this work are a simple criterion able to identify the situations where the pipe rack does not influence the high-pressure methane jet behavior, therefore allowing to identify the scenarios where simpler models can be used (*i.e.*, analytical correlations known for the free jet situation), and, if present, a simple analytical relationship that roughly predicts the influence of the pipe rack without the need of performing complex Computational Fluid Dynamics simulations.

## KEYWORDS

High-Pressure release; methane; pipe rack influence; risk assessment; CFD; analytical correlation

## ACRONYMS

CFD Computational fluid Dynamics

EDM Equivalent Diameter Model

FF Flash Fire

HP High-Pressure

LFL Lower Flammability Limit

ME Maximum Extent

NG Natural Gas

RANS Reynolds Averaged Navier-Stokes

UDF User Defined Function

## NOMENCLATURE

ABR: Area Blockage Ratio

$A_{ps}$: pseudo-source area extension

c: methane concentration in air

$c_{ax}$: methane concentration along the free jet axis

$C_D$: discharge coefficient

$C_p$: methane heat capacity

d: actual orifice diameter

D: pipe rack distance from the jet source

$d_{FJ}$: free jet diameter

$d_P$: rack pipes diameter

$d_{ps}$: pseudo-source orifice diameter

h: pipe rack case transversal beam height

H: pipe rack case height

$H_L$: pipe rack legs height

k: axial decay constant

L: pipe rack module extent

$\dot{m}_{ps}$: pseudo-source mass flow rate

ME: jet axial maximum extent

$ME_{FJ}$: free jet LFL cloud maximum extent in direction of the jet axis

$n_S$: shelves number

$n_{PS}$: number of pipes per shelf

p: upstream methane pressure

$p_{amb}$: environmental pressure

s: pipe rack case transversal beam width

T: upstream methane temperature

$T_{ps}$: methane static temperature at pseudo-source conditions

$T_{TOT,ps}$: methane total temperature at pseudo-source conditions

VBR: Volume Blockage Ratio

VFP: Vertical FootPrint

$v_{ps}$: methane velocity at pseudo-source conditions

W: pipe rack case width

α: pipe rack horizontal rotation with respect to the jet axis

γ: specific heat ratio

$\rho_{ps}$: methane density at pseudo-source conditions

$\rho_{amb}$: air density

# 1. INTRODUCTION

Although the diffusion of Natural Gas (NG, mainly constituted by methane) storage and transport under liquefied conditions, nowadays it is still common to have high pressure facilities using methane (or NG) in gaseous form in several industrial applications (Deng et al., 2018; Khraisheh et al., 2020).

This leads to several safety implications, related to both the High-Pressure (HP), at which the gas is stored, and its flammability. In particular, in case of late ignition, the release scenario can evolve into a Flash Fire (FF), whose hazardous distance is usually quantified as the Lower Flammability Limit (LFL) distance of the unignited cloud. Therefore, to predict how severe may be the consequences of a FF, the extension of the unignited flammable cloud needs to be estimated (Souza et al., 2019b). Commonly, in the risk analysis framework, for the case of a leakage of a

flammable substance such evaluation traduces in the prediction of the Maximum axially-oriented Extent (ME) of the cloud (Tchouvelev et al., 2007; Houf et al., 2010; Pontiggia et al., 2014; Colombini et al., 2020a).

Broadly speaking, two different situations of HP gaseous release can be identified: the free jet (intended as a release occurring in an unconfined environment (Dey et al., 2017) and the impinging jet (intended as a release interacting with structures or facilities in the surroundings (*i.e.*, obstacles) (Schefer et al., 2009).

For the latter, which can be expected to be the most probable accidental scenario in an industrial environment (Xu et al., 2011), it has been shown that, in some cases, an increase of the hazardous area (*i.e.*, the ME of the jet cloud) can occur (Kotchourko et al., 2014; Hall et al., 2017).

Despite this, in the past a large amount of the research in the process safety framework has been focused on the free jet scenario (e.g., Lockwood and Moneig (1980), Chen and Rodi (1980), Birch et al. (1984), Schefer and Dibble (1986); Birch et al. (1987), Becker et al. (1988), Pitts (1991), TNO (1997), Witlox and Holt (1999) and SHELL (2004)), while, for what concerns impinging jets, only recently some works have been performed with the aim of understanding how an obstacle can influence the jet behavior. In particular, Kim et al. (2013) investigated experimentally the self-ignition near an obstacle of HP hydrogen jets. Pontiggia et al. (2014) compared the performances of two different modeling approaches (namely, integral and Computational Fluid Dynamics (CFD) models) in predicting ME values for both impinged and non-impinged HP methane jets. Tolias and Venetsanos (2015), with the aim of giving best practices guidelines for hydrogen impinging jet simulations, investigated how to model an accidental impinging hydrogen jet through CFD models. Benard et al. (2016) investigated the effect of a near surface on the ME of high-pressure horizontal and vertical jets of both hydrogen and methane using CFD models. Gerbec et al. (2017) performed a CFD analysis of the release, and the subsequent environmental dispersion, of a vertical impinging propane jet out of an over-filled car tanker. Hall et al. (2017) investigated, both experimentally and numerically through CFD models, the ME of HP hydrogen jets impinging near surfaces. Uggenti et al. (2017) discussed the state-of-the-art of CFD models used for offshore installations risk assessments where impinging jets are usually involved: the aim was to compare the CFD benchmark case with the industrial standard. Hu et al. (2018) presented an improved version of the two-layer partitioning model based on the Abel-Noble equation of state (Johnston, 2005), which is able to predict more accurately the gas concentrations of HP under expanded hydrogen jets. The proposed model was applied to the flow of a horizontal HP hydrogen jet impacting a

vertical obstacle. Colombini and Busini (2019a and 2019b) investigated, using a CFD model, the accidental scenarios of an unignited HP methane jet impacting a horizontal and a vertical cylindrical tank to quantify the influence of some geometric parameters on the ME of the impinging jet. Colombini et al. (2020a and 2020b) investigated the effect of the ground (considered as a lateral impinging obstacle) on unignited methane high-pressure jets.

We can note that almost all the aforementioned works used CFD-based models. As discussed by Batt et al. (2016), Souza et al. (2019a), and Tolias et al. (2019), this is because only CFD-based numerical approaches are able to account properly for complex geometry. Therefore, although the high computational costs and the user knowledge demanded (Zuliani et al., 2016), CFD-based models are the most suitable numerical tools to model HP jet-obstacle scenarios and therefore they were used extensively in this work to provide useful insights in the HP methane jets-obstacle interaction.

In particular, going beyond the study of the simple interaction between a HP jet and a single well-shaped obstacle, this work investigated a credible, whilst probably rare, scenario, focusing on how a typical industrial structure (*i.e.*, a pipe rack) can influence the development of a HP methane jet in terms of ME of the flammable cloud. Through an extensive CFD-based analysis performed with Ansys Fluent 19.1 (Ansys Fluent User Guide, 2017), the main geometrical parameters on which the impinging jet behavior depends were identified allowing for developing a simple analytical relationship that roughly predicts the influence of the pipe rack without the need of performing complex CFD simulations. Moreover, a simple criterion able to identify the situations where the pipe rack does not influence the HP methane jet behavior was developed, therefore allowing to identify the scenarios where simpler models (*e.g.*, analytical correlations able to estimate the ME of a free jet) can be used. Both these outcomes can be quite valuable for practitioners daily involved in industrial safety assessments.

## 2. MATERIALS AND METHODS

The commercial platform Ansys Workbench v. 19.1 (Ansys Workbench User Guide, 2017) was used to model, through a CFD approach, an unignited HP methane jet impinging a pipe rack.

The computational domain was created with Ansys DesignModeler, the grid was built using Ansys Meshing and the computations were performed with the numerical solver Ansys Fluent (Ansys Workbench User Guide, 2017; Ansys DesignModeler User Guide, 2017; Ansys Meshing User Guide, 2017; Ansys Fluent User Guide, 2017).

Moreover, as usually done when modeling HP jets in the safety assessment field (*e.g.,* Hess et al., 1973; Sposato et al., 2003; Pontiggia et al., 2014; Benard et al., 2007; Houf et al., 2007; Stewart et al., 2019; Tolias et al., 2019), instead of simulating through the CFD also the early stage of the jet development (*i.e.*, the so-called nearfield zone of the jet), the Equivalent Diameter Model (EDM) approach was (Franquet et al., 2015); in particular, the EDM proposed by Birch et al. (1984) was used, as discussed in the following section.

# 3. SCENARIO DESCRIPTION

The scenario analyzed in this work mimes an industrial situation involving a horizontally oriented high-pressure release of methane impinging a pipe rack as sketched in Figure 1, where also the relevant geometric dimensions are labelled.

The methane source was modelled as a nozzle while the pipe rack was represented by a rectangular structure housing several pipes far from the ground. The HP jet nozzle was located at 4.85 m above the ground (which corresponds to the mid-height of the pipe case). 5D atmospheric conditions (*i.e.*, a wind intensity of 5 m/s at 10 m from the ground and a Pasquill stability class of D) with the wind blowing alongside and in the same direction of the jet were considered. To properly model such wind conditions, the inlet velocity profile was provided as input to the numerical solver through an *ad hoc* User Defined Function (UDF).

To investigate how the HP jet development is influenced by the rack, several parameters (related to both the jet source and the obstacle) were considered, namely: upstream methane pressure (p); actual orifice diameter of the jet source (d); rack pipes diameter ($d_p$); shelves number ($n_s$); number of pipes per shelf ($n_{PS}$); rack distance from the jet source (D); pipe rack horizontal rotation with respect to the jet axis (α). Moreover, also the target concentration considered in relation to the ME of the jet (c) was varied in order to see how the jet development modifies when different concentrations are of interest.

As previously mentioned, since the early stage of the jet development was modelled using the EDM approach proposed by Birch et al. (1984), to include all the physical phenomena on one hand and to avoid any unwanted interference of the boundaries on the other, the domain extents were defined through some preliminary tests, resulting in a rectangular box of 100 m length, 25 m height and 15 m wide. Note that 15 m is half the width of the domain, thanks to the symmetry of the geometry; in the few cases where no symmetry plane is present, a 30 m width was used.

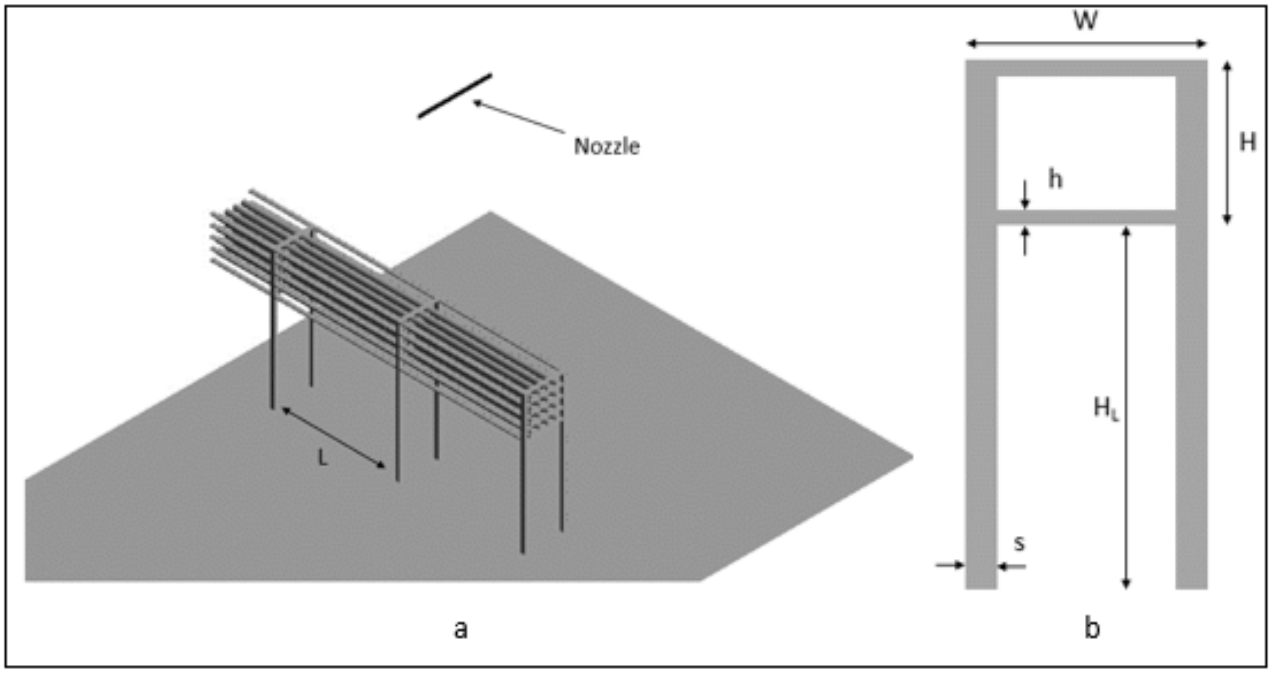


Fig. 1: Scenario configuration: a) whole appearance, b) pipe rack structure details. Figure 1b reports the relevant dimensions of the rack structure that were kept the same in all the analysis: s = 0.15 m, h = 0.05 m, H = 1.7 m, $H_L$ = 4 m, W = 1.75 m, L = 5 m. The scenario that is shown is symmetric with respect to the vertical plane crossing the jet axis.

The strategy used for the mesh deployment is discussed in detail elsewhere (Colombini et al. (2020a)). In particular, the *body of influence* feature was used to thicken the computational grid in a volume surrounding the jet axis (which is the computationally critical zone), allowing a less dense mesh close to the domain boundaries (where demanding physical phenomena are not expected). To properly model the flow-rack interaction, the *inflation* mesh feature was applied to the surfaces of the obstacle to achieve an adequate boundary layer discretization (Ansys Meshing User Guide, 2017). In the investigated conditions, the flow interacting with a solid surface cohabits with regions in which the turbulent flow does not interact with any solid surface. To correctly model both the situations and, at the same time, to limit the computational costs, the Reynolds Averaged Navier-Stokes (RANS) approach was adopted and coupled with the two-equation eddy-viscosity k-ω SST turbulence closure model (Menter, 1993). Figure 2 shows, for one of the cases investigated (run 12 in Table 3), the resulting full-tetrahedral mesh. Depending on the specific case considered (which is related to the values of the parameters involved) the number of cells ranged from 8 to 18 million. Quality requirements (*i.e.*, skewness and orthogonal quality) were always verified. Moreover, for a reference case (run 12 in Table 3), the independence of the results from the grid

was qualitatively and quantitatively verified in terms of concentration and velocity decay in correspondence of the symmetry vertical plane, by halving and doubling the elements size of the body of influence features. Figure 1S in the supplementary material shows the comparison of the sensitivity analysis results in terms of methane mole fraction in air and velocity contours.

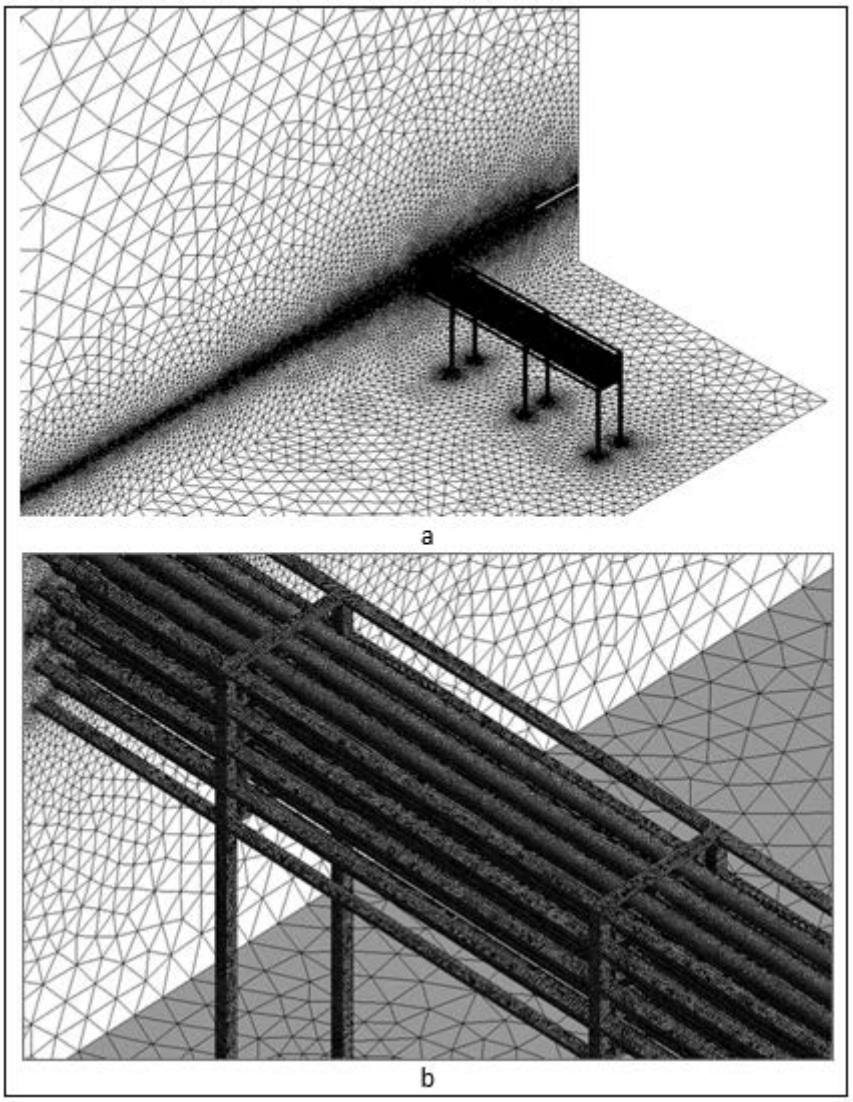


Fig. 2: General view of the surface grid (a) and its detail in proximity to the pipe rack (b).

All simulations were accrued out in steady-state conditions and the use of the EDM to simulate the near zone of the jet allowed the flow to be treated as incompressible. For this reason, the pressure-based solver was used. To account for the multi-species problem (methane release in ambient air), the species transport model with no reaction was selected. The fluid system was considered as an ideal gaseous mixture, and density was modelled by means of the ideal gas Equation of State. Gravity acceleration was always included perpendicularly to the ground surface.

The second order upwind spatial-discretisation scheme was considered for all the convective terms and the COUPLED pressure-velocity coupling scheme was adopted. Table 1S in the supplemental information lists the model equations together with the definition of the main parameters.

Using the methane upstream conditions and the actual nozzle diameter considered, the equivalent jet source boundary conditions were computed, case by case, with the Birch et al. (1984) model. Table 1 reports the equations defining the pseudo-source characteristics used for the methane jet inlet. The other boundary conditions were kept unchanged for all the cases and they are summarized in Table 2.

Table 1: Equations of the Birch et al. (1984) model defining the pseudo-source characteristics of the methane jet inlet.

| Pseudo-source characteristic | Equation |
|---|---|
| Equivalent diameter | $d_{ps} = d\sqrt{C_D\left(\frac{p}{p_{amb}}\right)\left(\frac{2}{\gamma+1}\right)^{\frac{(\gamma+1)}{2(\gamma-1)}}}$ |
| Mass flow rate | $\dot{m}_{ps} = \rho_{ps} \cdot A_{ps} \cdot v_{ps}$ |
| Total temperature | $T_{TOT,ps} = T_{ps} + \frac{v_{ps}^2}{2\,c_p}$ |

Table2: Boundary conditions assignments.

| Boundary name | Type | Specifics |
|---|---|---|
| Wind inlet | Velocity inlet | air, $v_z$ = UDF velocity profile, T = 300 K |
| Top boundary | Velocity inlet | air, $v_z$ = 5.5 m/s, T = 300 K |
| Left boundary | Velocity inlet | air, $v_z$ = UDF velocity profile, T = 300 K |
| Ground | Wall | 0.01 m roughness height, adiabatic |
| Symmetry | Symmetry | - |
| Wind outlet | Pressure outlet | air, $T_{BACKFLOW}$ = 300 K |
| Pipe nozzle | Wall | 0.001 m roughness height, adiabatic |
| Methane jet inlet | Mass flow inlet | Computed case by case with Birch et al. (1984) model. See Table 1. |
| Pipe rack | Wall | 0.001 m roughness height, adiabatic |

Three dimensionless parameters were used to summarize the HP jet-rack interaction, as detailed in the following equations as well as in Figures 3, 4 and 5:

$$VBR = \frac{n_{PS} \cdot n_S \cdot \frac{\pi \cdot d_P^2}{4} + 2 \cdot (n_S + 1) \cdot s \cdot h}{H \cdot W} \quad (1)$$

$$ABR = \frac{h \cdot (n_S + 1) + d_P \cdot n_S}{H} \quad (2)$$

$$VFP = \frac{d_{FJ}(D)}{H} \tag{3}$$

All the parameters involved in these equations are already defined in Figure 1 apart from $d_{FJ}(D)$ that is the free jet diameter evaluated in correspondence of the pipe rack position (see Figure 5). VBR (which stands for Volume Blockage Ratio, that is the ratio between occupied rack case volume and full rack case volume – see Figure 3) indicates how the volume within the rack case is occupied by pipes and structural beams; ABR (which stands for Area Blockage Ratio, that is the ratio between occupied rack case frontal area and full rack case frontal area – see Figure 4) indicates how the frontal area of the rack case is hindered by pipes and structural beams; VFP (which stands for Vertical FootPrint, that is the hypothetical free jet footprint on the pipe rack - see Figure 5) indicates whether the free jet cloud radial extent (at the considered concentration level) is larger than (or smaller) the height of the rack case.

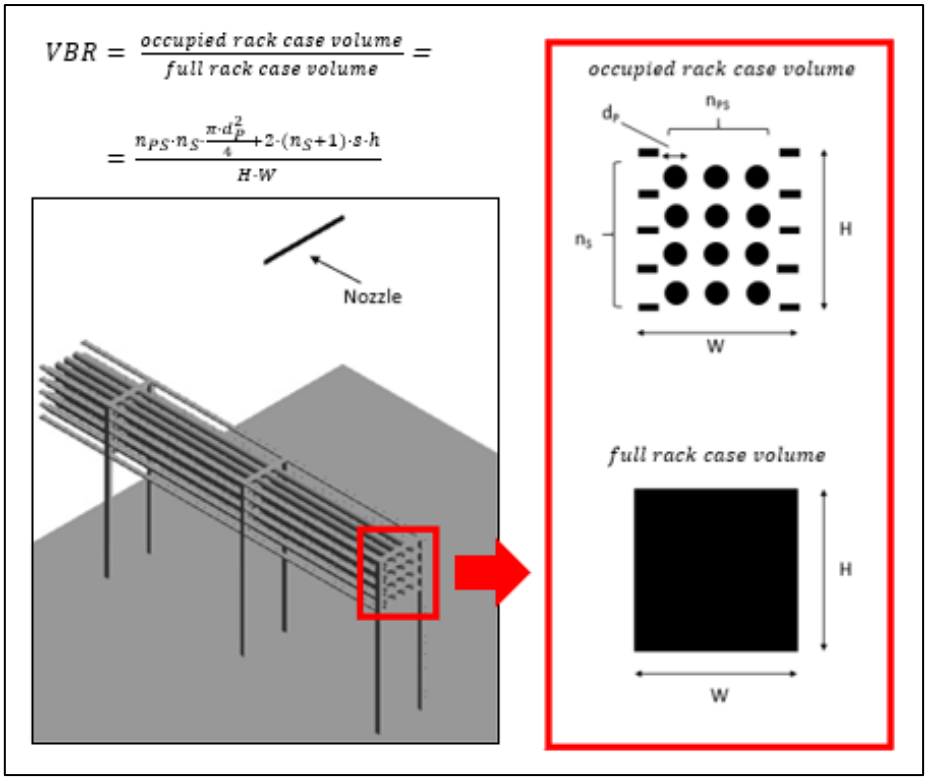


Fig. 3: Physical meaning of VBR.

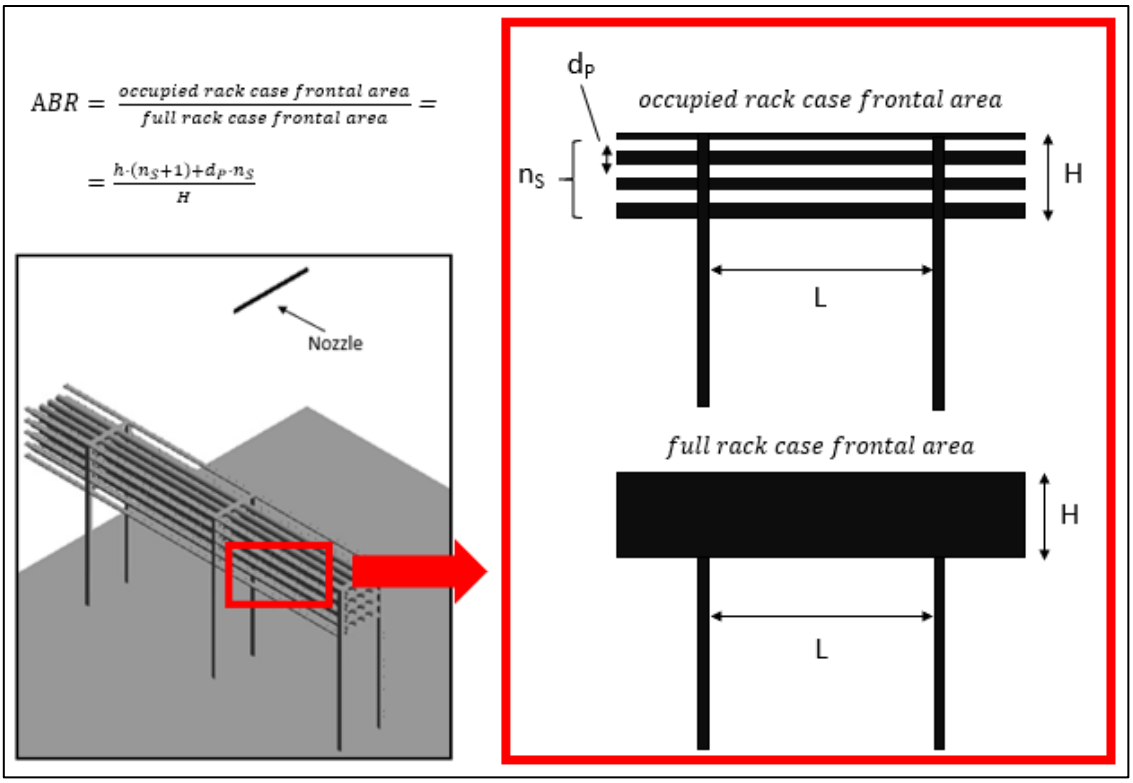


Fig. 4: Physical meaning of ABR.

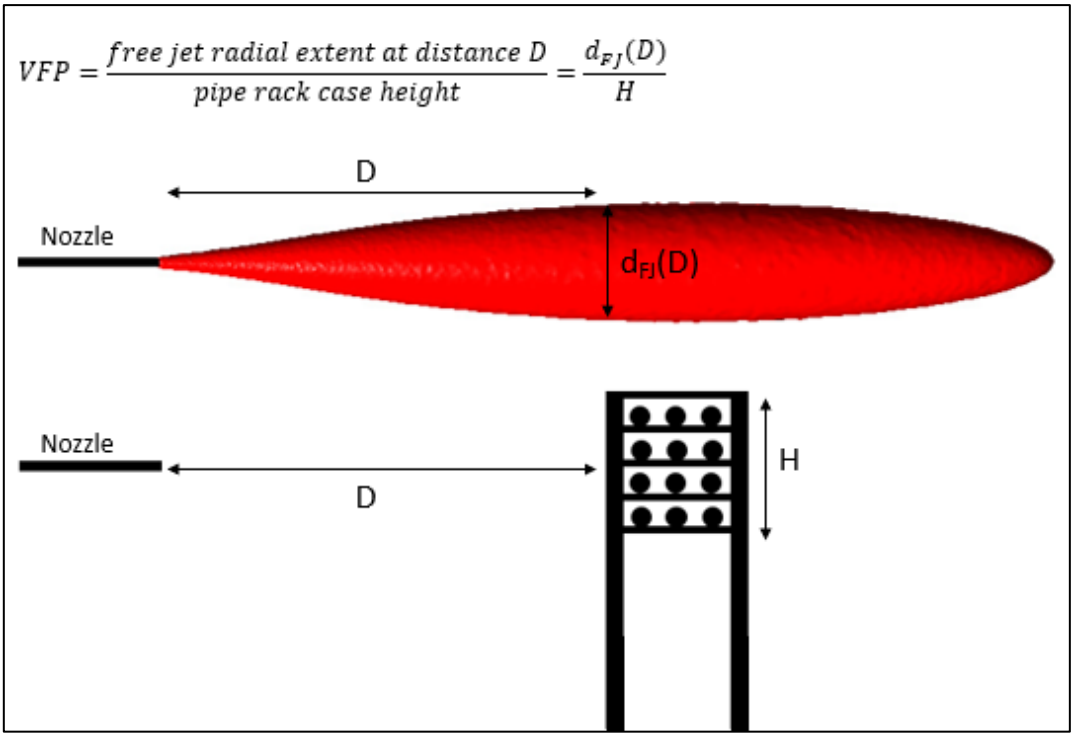


Fig. 5: Physical meaning of VFP.

# 4. RESULTS

At first, the geometrical characteristics of the pipe rack (namely: $d_p$, $n_s$, and $n_{PS}$) were changed within realistic ranges, as shown in Table 3, while the values of all the other parameters were kept unchanged: p = 65 bar, T = 278 K, d = 0.0254 m, D = 7.68 m (*i.e.*, half of ME of a free jet at methane LFL), α = 0° (that is, the pipe rack is perpendicular to the jet axis) and c = 5.3 % (methane LFL).

Table 3: Values of the characteristics defining the cases simulated.

| **Run** | $d_p$ [m] | $n_{PS}$ | $n_s$ | | **Run** | $d_p$ [m] | $n_{ps}$ | $n_s$ |
|---|---|---|---|---|---|---|---|---|
| **1** | 15.19 | 2 | 3 | | **20** | 25 | 4 | 3 |
| **2** | 21.48 | 2 | 3 | | **21** | 26.31 | 4 | 3 |
| **3** | 25 | 2 | 3 | | **22** | 15.19 | 5 | 3 |
| **4** | 26.31 | 2 | 3 | | **23** | 21.48 | 5 | 3 |
| **5** | 30.38 | 2 | 3 | | **24** | 25 | 5 | 3 |
| **6** | 33.97 | 2 | 3 | | **25** | 15.19 | 3 | 4 |
| **7** | 37.21 | 2 | 3 | | **26** | 21.48 | 3 | 4 |
| **8** | 15.19 | 3 | 3 | | **27** | 25 | 3 | 4 |
| **9** | 17.54 | 3 | 3 | | **28** | 15.19 | 4 | 4 |
| **10** | 21.48 | 3 | 3 | | **29** | 21.48 | 4 | 4 |
| **11** | 24.81 | 3 | 3 | | **30** | 28 | 4 | 4 |
| **12** | 25 | 3 | 3 | | **31** | 15.19 | 3 | 5 |
| **13** | 26.31 | 3 | 3 | | **32** | 21.48 | 3 | 5 |
| **14** | 27.74 | 3 | 3 | | **33** | 25 | 3 | 5 |
| **15** | 30.38 | 3 | 3 | | **34** | 15.19 | 4 | 5 |
| **16** | 15.19 | 4 | 3 | | **35** | 21.48 | 4 | 5 |
| **17** | 18.61 | 4 | 3 | | **36** | 15.19 | 3 | 6 |
| **18** | 21.48 | 4 | 3 | | **37** | 21.48 | 3 | 6 |
| **19** | 24.02 | 4 | 3 | | **38** | 15.19 | 4 | 6 |

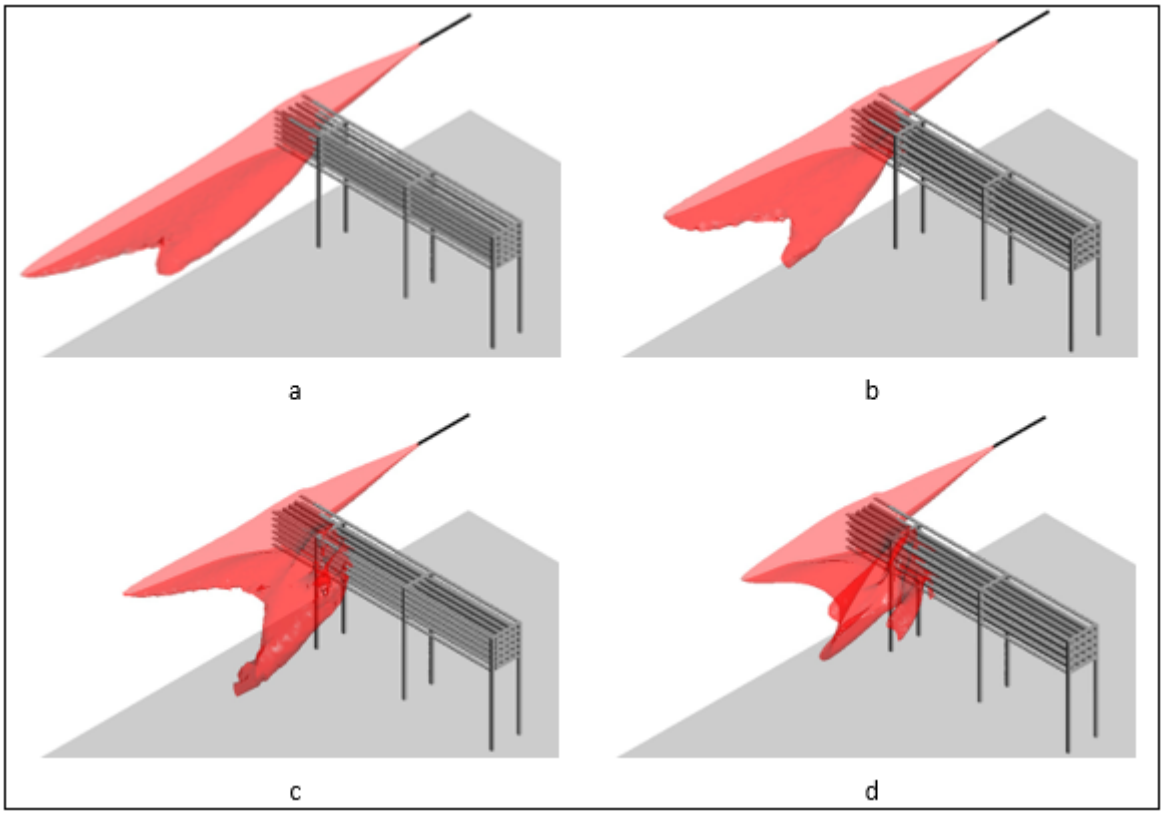


Fig. 6: Isosurfaces of methane concentration in air equal to 5.3% for some of the runs in Table 2: a) run 31, b) run 29, c) run 35 and d) run 30.

As an example, Figure 6a-d shows the isosurfaces of some of the runs listed in Table 3. Qualitatively, we can see that, in all the cases, the jet cloud passes over the rack structure, even if the ME of the LFL is not always located along the jet axis. Comparing Figure 6b and 6d we can see that an increase in the pipes diameter results in a reduction of the ME together with a lateral enlargement of the cloud. Comparing Figure 6b and 6c we can see that increasing the number of pipes per shelf leads to an overall ME reduction and to a more enhanced split of the jet cloud.
These behaviours can be recast in terms of VBR and ABR values considering runs 30 and 31 (which show the same VFP = 1.09 value and an VBR·ABR value about 4 times larger for run 30 than run 31) together with the free jet simulation, as shown in Figure 7.

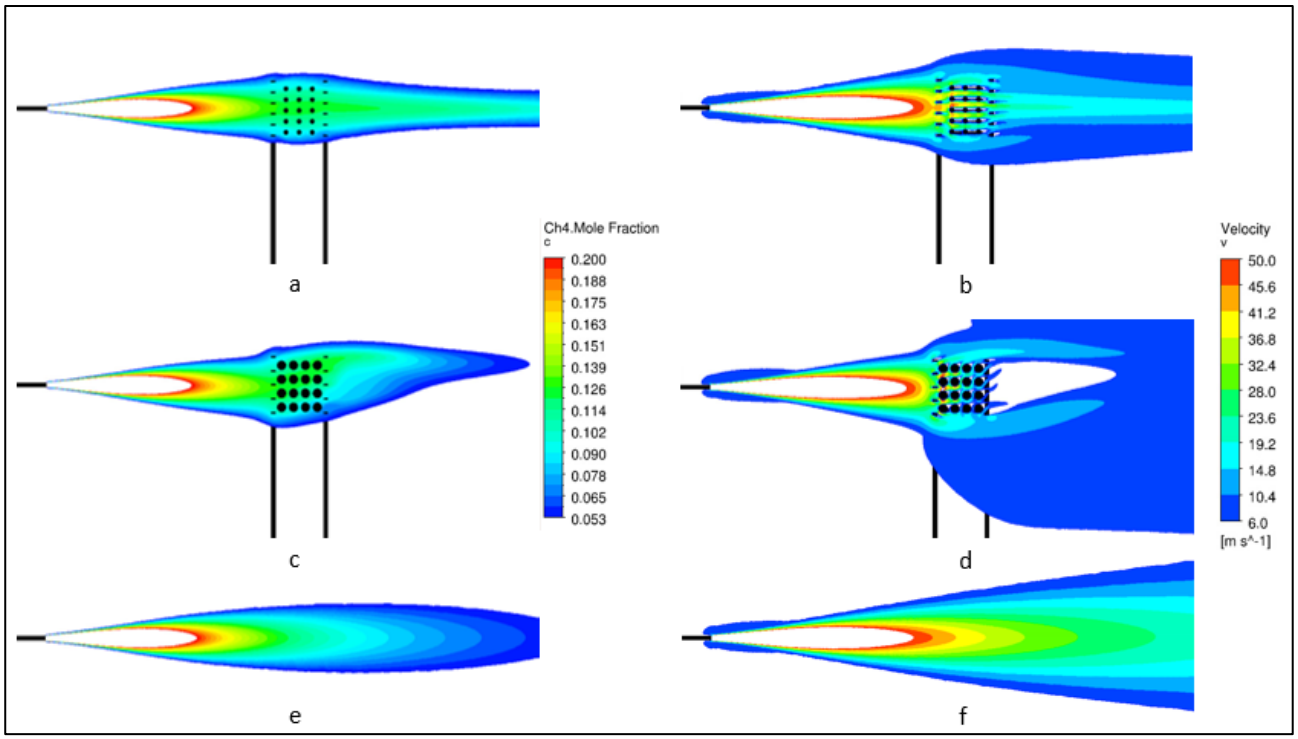


Fig. 7: Contours of methane concentration in air and flow velocity in correspondence of the domain vertical symmetry plane for two runs of Table 2 (Figure 7a-b run 31, Figure 7c-d run 30) and for the free jet situation (Figure 7e-f). For run 31 VBR·ABR = 0.075 and ME = 23.7 m, while, for run 30 VBR·ABR = 0.287 and ME = 14.68 m.

Comparing Figures 7a and 7c with Figure 7e we can see that the obstacle acts as a sort of isolating structure able to reduce the jet air entrainment; as a matter of fact, the methane concentration does not decrease when the jet passes through the rack case. Moreover, the jet velocity immediately downstream the rack case is lower than that in free jet conditions, limiting the dilution effect caused by the velocity difference with the bulk fluid (see Figures 7b and 7d with respect to Figure 7f). The combination of these two phenomena leads to longer jet clouds. We can also see that when both the front area of the obstacle and the volume within it are less hindered by the pipes the aforementioned physical phenomena are more relevant leading to longer jet cloud when either VBR or ABR decreases. However, when VBR and ABR reduced to very low values, the pipe rack looks like more to an empty volume rather than an obstacle, therefore allowing the jet to pass through the obstacle undisturbed. In these conditions the impinging jet is expected to approximate the free jet behaviour.

All these results can be rationalized as shown in Figure 8, where the ratio of the LFL cloud ME computed for all the runs in Table 3 to the LFL cloud ME computed for a corresponding free jet ($ME_{FJ}$, that is, the LFL cloud ME computed for the same jet without any obstacle interaction) is reported as a function of the product of the three aforementioned dimensionless parameters

(note that the $ME_{FJ}$ value can be easily estimated using well known analytical correlations, *e.g.*, Chen and Rodi (1980)).

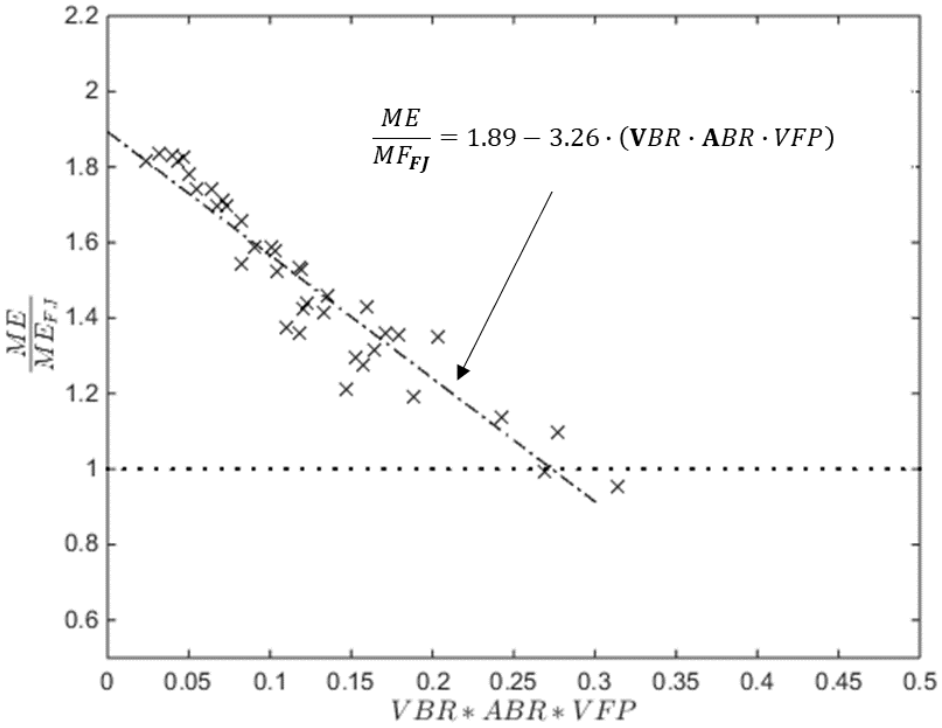


Fig. 8: Dimensionless space defined exploiting the dimensionless parameters introduced in Section 3. X markers are the results computed for the 38 runs listed in Table 3, the dotted line represents ME = $ME_{FJ}$ ($ME_{FJ}$ = 15.37 m) while the dashed-dotted line is the linear fitting of the computed data.

From this Figure we can see a clear trend showing how the rack influences the jet development: ME of the LFL jet cloud is always larger than (or almost equal to) $ME_{FJ}$. This means that the rack is never able to reduce the LFL jet ME; in the worst case, the ME of the free jet is almost doubled by the presence of the rack. Moreover, the following linear interpolation of the results provides a reasonable fitting:

$$\frac{ME}{MF_{FJ}} = 1.89 \ - 3.26 \cdot (VBR \cdot ABR \cdot VFP) \tag{4}$$

with a percentage error, defined as $\epsilon = \frac{\Sigma_{i=1}^{n}\left(\frac{|y_i - y|}{y_i}\right)}{n} \cdot 100$ (where $y_i$ is the ratio between ME and $ME_{FJ}$ computed for each run, y the ratio between ME and $ME_{FJ}$ computed with Equation 4 and n=38 is the number of runs), equal to 4.4 %.

Starting from the conditions of run 12 in Table 3, several different scenarios were investigated, varying p, d, D, α, and c, as summarized in Table 4. Results of runs 39-126 are shown in Figure 9, where the same plan of Figure 8 was used. Notice that, targeting to highlight the influence of only the observed methane concentration, runs 51-126 replicated twice the 38 runs detailed in Table 3, keeping methane source conditions of run 12 and varying the methane concentration observed (c = 2.65 % for runs 51-88 and 10 % for runs 89-126).

Table 4: Characteristics defining the scenarios targeting to generalize the analytical correlation.

| **Run** | p [bar] | d [m] | D [m] | α [°] | c [%] |
|---|---|---|---|---|---|
| **39** | 32.5 | 0.0254 | 7.68 | 90 | 5.3 |
| **40** | 130 | 0.0254 | 7.68 | 90 | 5.3 |
| **41** | 65 | 0.0127 | 7.68 | 90 | 5.3 |
| **42** | 65 | 0.0508 | 7.68 | 90 | 5.3 |
| **43** | 65 | 0.0254 | 3.84 | 90 | 5.3 |
| **44** | 65 | 0.0254 | 5.76 | 90 | 5.3 |
| **45** | 65 | 0.0254 | 9.6 | 90 | 5.3 |
| **46** | 65 | 0.0254 | 11.52 | 90 | 5.3 |
| **47** | 65 | 0.0254 | 13.44 | 90 | 5.3 |
| **48** | 65 | 0.0254 | 15.36 | 90 | 5.3 |
| **49** | 65 | 0.0254 | 7.68 | 112.5 | 5.3 |
| **50** | 65 | 0.0254 | 7.68 | 135 | 5.3 |
| **51-88** | 65 | 0.0254 | 7.68 | 90 | 2.65 |
| **89-126** | 65 | 0.0254 | 7.68 | 90 | 10 |

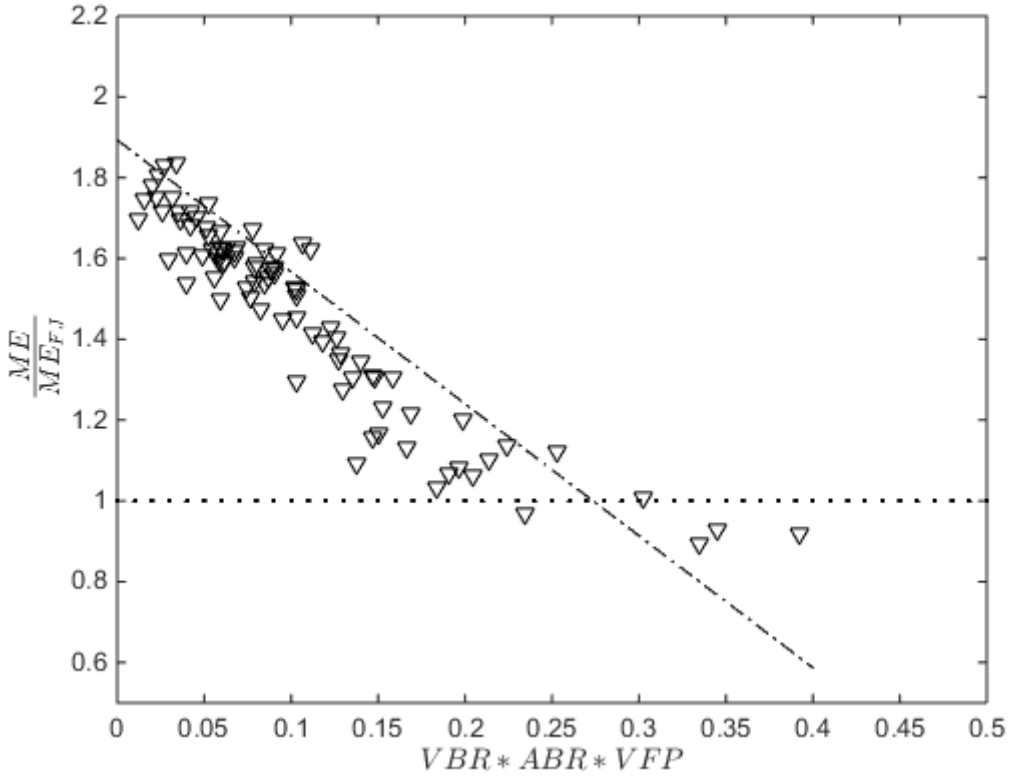


Fig.9: Results of runs in Table 4 are shown in the plan defined in Figure 8. The flipped triangular markers are the results computed for the 88 runs listed in Table 4, the dotted line represents ME = $ME_{FJ}$ ($ME_{FJ}$ = 15.37 m) while the dashed-dotted line is the linear fitting of the computed data (Eq. 4).

We can see that the linear correlation deduced from the fitting of the first 38 runs (Eq. 4) is able to represent reasonably well also the results of the new 88 runs, with a mean percentage error equal to 7.8. This is an important evidence supporting the reliability of the proposed correlation.

Considering the 126 scenarios analysed we can see that only a few of them present a value of VBR·ABR·VFP greater than 0.3 and they show a value of $ME/ME_{FJ}$ around one. This leads to the inference that for values of VBR·ABR·VFP larger than 0.3 the obstacle expires its influence on the jet development.

To confirm this inference four *ad hoc* runs were investigated, as summarized in Table 5. The results obtained for these four runs are summarized in Figure 10 together with the results of all the previous runs. Notice that, run 130 is intended to resemble a pipe rack with a high filling degree of both case volume (VBR) and front area (ABR). To do so, a horizontal cylinder with a diameter equal to the rack case height, H, and placed in the same position of the pipe rack was used as extreme situation.

Table 5: Characteristics defining the scenarios targeting to obtain large values of VBR·ABR·VFP.

| Run | p [bar] | d [m] | D [m] | α [°] | c [%] | $d_p$ [m] | $n_{PS}$ | $n_s$ | VBR [-] | ABR [-] | VFP [-] | VBR·ABR·VFP [-] |
|---|---|---|---|---|---|---|---|---|---|---|---|---|
| **127** | 65 | 0.0254 | 7.68 | 90 | 5.3 | 21.48 | 4 | 6 | 0.33 | 0.96 | 1.09 | 0.345 |
| **128** | 65 | 0.0254 | 7.68 | 90 | 5.3 | 32 | 4 | 4 | 0.46 | 0.90 | 1.09 | 0.450 |
| **129** | 65 | 0.0254 | 7.68 | 90 | 5.3 | 22 | 6 | 6 | 0.50 | 0.98 | 1.09 | 0.532 |
| **130** | 65 | 0.0254 | 7.68 | 90 | 5.3 | 1.7 | 1 | 1 | 0.76 | 1 | 1.09 | 0.830 |

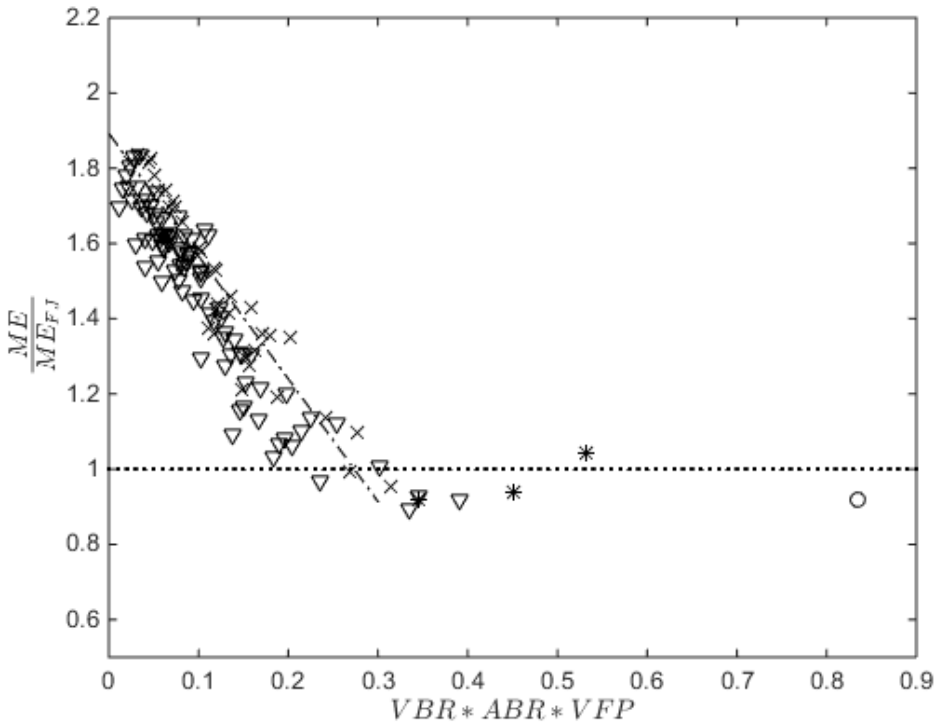


Fig.10: Results of runs listed in Table 5 are added to Figure 9 to show what occurs for large values of VBR·ABR·VFP. Moreover, also results in Figure 8 have been reported. X markers are the results computed for the 38 runs listed in Table 3, flipped triangular markers are the results computed for the 88 runs listed in Table 4, asterisk markers are the results computed for the 3 pipe rack cases listed in Table 5 (first three rows of the Table), circle marker is the result computed for the single horizontal cylinder case in Table 5 (last row of the Table), the dotted line represents ME = $ME_{FJ}$ ($ME_{FJ}$ = 15.37 m) while the dashed-dotted line is the linear fitting of the computed data (Eq. 4).

We can see that also for VBR·ABR·VFP much larger than 0.3 values of $ME/ME_{FJ}$ around one were obtained. The reason is that an increase in VBR or ABR results in an obstacle with a high degree of volume filled by pipes, therefore decreasing the possibility to the methane jet of passing through it. The jet is therefore more and more forced to travel around the obstacle, leading to a ME of the jet close to that of a free jet.

# 5. DISCUSSION

Based on the results achieved and detailed in previous Section, the main findings of this work can be summarized in the following procedure, which allows estimating the ME of a methane flammable jet cloud impinging a pipe rack without any demanding CFD-based computation (in terms of both time and analyst skill):

1. From both the obstacle and source characteristics, estimate VBR, ABR, and VFP values (as detailed in Section 3):

$$VBR = \frac{n_{PS} \cdot n_S \cdot \frac{\pi \cdot d_P^2}{4} + 2 \cdot (n_S + 1) \cdot s \cdot h}{H \cdot W}$$

$$ABR = \frac{h \cdot (n_S + 1) + d_P \cdot n_S}{H}$$

$$VFP = \frac{d_{FJ}(D)}{H}$$

to analytically estimate $d_{FJ}(D)$, the following models need to be used:

$$d_{FJ}(D) = 2 \cdot \sqrt{-\frac{D^2}{50} \cdot \ln\left(\frac{\bar{c}}{c_{ax}(D)}\right)}$$ Cushman-Roisin (2020)

$$c_{ax}(D) = \frac{k d_{ps}}{D}\left(\frac{\rho_{amb}}{\rho_{ps}}\right)^{\frac{1}{2}}$$ Chen and Rodi (1980)

where D is the pipe rack distance from the jet source, $\bar{c}$ is the specific methane concentration in air considered, $c_{ax}(D)$ is the methane concentration along the free jet axis computed at a distance D from the jet source, k is the axial decay constant (4.4 (Birch et al. (1984)), $d_{ps}$ is the pseudo-source orifice diameter (computed with the model of Birch et al. (1984)), $\rho_{amb}$ is the air density (computed at the ambient conditions), $\rho_{ps}$ is the methane density at pseudo-source conditions. To show the capability of the previous analytical models to provide a reasonable prediction of $d_{FJ}(D)$, Figure 2S in the supplementary material compares the radial extent of a given free jet computed with the CFD model and the previous analytical ones.

2. From the source characteristics, estimate the $ME_{FJ}$ value using the Chen and Rodi (1980) concentration decay model:

$$ME_{FJ} = \frac{kd_{ps}}{LFL}\left(\frac{\rho_{amb}}{\rho_{ps}}\right)^{\frac{1}{2}}$$

Notice that, the Chen and Rodi (1980) model reliability in estimating $ME_{FJ}$ is discussed in detail in the work of Colombini et al. (2020a).

3. If VBR·ABR·VFP > 0.3, $ME_{FJ}$ provides the order of magnitude of ME
4. If VBR·ABR·VFP < 0.3, the order of magnitude of ME can be estimated as

$$\frac{ME}{MF_{FJ}} = 1.89 - 3.26 \cdot (VBR \cdot ABR \cdot VFP)$$

Finally, it should be stressed that this procedure is expected to provide a reasonable estimation as an order of magnitude of ME for methane HP jets inside the parameters window investigated. The use of detailed CFD simulations should be always considered both for confirming the estimated values, as well as for obtaining more reliable estimation either in highly sensitive scenarios or in scenarios characterized by parameter values outside the investigated window. Future works could focus to extent the validity of the proposed procedure considering different rack configurations or even analysing if the proposed procedure can be applied to scenarios involving different substances.

# 6. CONCLUSIONS

The impinging high-pressure jet release of methane can be a relevant scenario in several industrial facilities. Among the others, the credible, whilst probably rare, scenario involving the impingement of a pipe rack was deeply investigated through a CFD-based model, showing that the presence of a rack either enhance (for VBR· ABR·VFP lower than about 0.3, see Figure 10) or does not influence (for VBR·ABR·VFP larger than about 0.3, see Figure 10) the ME of the flammable jet with respect to the free jet. In particular, as practical tool for daily risk assessment activities, this work proposes a by hand procedure allowing the estimation of the maximum axial extent of jet cloud.

# COMPETING INTERESTS STATEMENT

The Authors declare that there is no conflict of interest.

## ACKNOWLEDGEMENTS

This research did not receive any specific grant from funding agencies in the public, commercial, or not-for-profit sectors.

## REFERENCES

Ansys DesignModeler User's Guide, 2017. Release 19.0. ANSYS, Inc.

Ansys Fluent User's Guide, 2017. Release 19.0. ANSYS, Inc.

Ansys Meshing User's Guide, 2017. Release 19.0. ANSYS, Inc.

Ansys Workbench User's Guide, 2017. Release 19.0. ANSYS, Inc.

Batt, R., Gant, S.E., Lacome, J.M., Truchot, B., 2016. Modelling of stably-stratified atmospheric boundary layers with commercial CFD software for use in risk assessment. *Chem. Eng. Trans.* 48, 61–66. https://doi.org/10.3303/CET1648011.

Becker, H.A., Cho, S.H., Ozum, B., Tsujikawa, H., 1988. Turbulent mixing in the impingement zone of dual opposed free jets and of the normal wallimpinging jet. *Chem. Eng. Commun*. 67, 291-313. http://dx.doi.org/10.1080/00986448808940390

Bénard, P., Tchouvelev, A., Hourri, A., Chen, Z., Angers, B., 2007. High pressure hydrogen jets in the presence of a surface. *Int. Conf. Hydrog. Saf.* 40.

Bénard, P., Hourri, A., Angers, B., Tchouvelev, A., 2016. Adjacent surface effect on the flammable cloud of hydrogen and methane jets: Numerical investigation and engineering correlations. *Int. J. Hydrogen Energy* 41, 18654–18662. https://doi.org/10.1016/j.ijhydene.2016.08.173.

Birch, A.D., Brown, D.R., Dodson, M.G., Swaffield, F., 1984. The structure and concentration decay of high pressure jets of natural gas. *Combust. Sci. Technol.* 36, 249–261. https://doi.org/10.1080/00102208408923739.

Birch, A.D., Hughes, D.J., Swaffield, F., 1987. Velocity decay of high pressure jets. *Combust. Sci. Technol.* 52, 161-171. http://dx.doi.org/10.1080/00102208708952575

Chen, C.J., Rodi, W., 1980. Vertical Turbulent Buoyant Jets – A review of Experimental Data, First ed. Pergamon Press Vol. 4.

Colombini, C., Busini, V., 2019a. Obstacle Influence on High-Pressure Jets based on Computational Fluid Dynamics Simulations. *Chem. Eng. Trans.* 77, 811–816. https://doi.org/10.3303/CET1977136.

Colombini, C., Busini, V., 2019b. High-Pressure Methane Jet: Analysis of the Jet-Obstcle Interaction. *Proceeding of the 29th European Safety and Reliability Conference.*

Colombini, C., Martani, A., Rota, R., Busini, V., 2020a. Ground influence on high-pressure methane jets: Practical tools for risk assessment. *J. Loss Prevent. Proc.* 67, 104240. https://doi.org/10.1016/j.jlp.2020.104240

Colombini, C., Carlini, L., Rota, R., Busini, V., 2020b. Ground Interaction on High-Pressure Jets: Effect on Different Substances. *Chem. Eng. Trans.* 83. To be printed.

Cushman-Roisin, B., Environmental Fluid Mechanics – John Wiley & Sons, Book in preparation. Last online access: August 2020. http://www.dartmouth.edu/~cushman/books/EFM/chap9.pdf

Deng, Y., Hu, H., Yu, B., Sun, D., Hou, L., Liang, Y., 2018. A method for simulating the release of natural gas from the rupture of high-pressure pipelines in any terrain. *J. Hazard. Mater.* 342, 418–428. https://doi.org/10.1016/j.jhazmat.2017.08.053.

Dey, S., Kishore, G.R., Castro-Orgaz, O., Ali, S.Z., 2017. Hydrodynamics of submerged turbulent plane offset jets. *Phys. Fluids* 29. https://doi.org/10.1063/1.4989559.

Franquet, E., Perrier, V., Gibout, S., Bruel, P., 2015. Free underexpanded jets in a quiescent medium: A review. *Prog. Aerosp. Sci.* 77, 25–53. https://doi.org/10.1016/j.paerosci.2015.06.006.

Gerbec, M., Pontiggia, M., Antonioni, G., Tugnoli, a., Cozzani, V., Sbaouni, M., Lelong, R., 2017. Comparison of UDM and CFD simulations of a time varying release of LPG in geometrical complex environment. *J. Loss Prev. Process Ind.* 45, 56–68. https://doi.org/10.1016/j.jlp.2016.11.020.

Hall, J.E., Hooker, P., O'Sullivan, L., Angers, B., Hourri, A., Benard, P., 2017. Flammability profiles associated with high-pressure hydrogen jets released in close proximity to surfaces. *Int. J. Hydrogen Energy* 42, 7413–7421. https://doi.org/10.1016/j.ijhydene.2016.05.113.

Hess, K., Leukel, W., Stoeckel, A., 1973. Formation of explosive clouds on overhead release and preventive measure. *Chemie-Ingenieur-Technik* 45, 5.

Houf, W., Schefer, R., 2007. Predicting Radiative Heat Flux and Flammability Envelopes from Unintended Releases of Hydrogen. *Int. J. Hydrogen Energ.* 32, 136-151. https://doi.org/10.1016/j.ijhydene.2006.04.009

Houf, W., Schefer, R., Evans, G., Merilo, E., Groethe, M., 2010. Evaluation of barrier walls for

mitigation of unintended releases of hydrogen. *Int. J. Hydrogen Energy* 35, 4758–4775. https://doi.org/10.1016/j.ijhydene.2010.02.086.

Hu, J., Christopher, D.M., Li, X., 2018. Simplified partitioning model to simulate high pressure under-expanded jet flows impinging vertical obstacles. Int. J. Hydrogen Energ. 43, 13649-13658. https://doi.org/10.1016/j.ijhydene.2018.05.036

Jhonston, I.A., 2005. The Noble-Abel Equation of State: Thermodynamic Derivations for Ballistics Modelling. *Weapons Systems Division Defence Science and Technology Organisation*. DSTO-TN-0670.

Khraisheh, M., Almomani, F., Walker, G., 2020. Solid Sorbents as a Retrofit Technology for CO2 Removal from Natural Gas Under High Pressure and Temperature Conditions. *Sci. Rep.* 10, 269. https://doi.org/10.1038/s41598-019-57151-xx

Kim, S., Lee, H.J., Park, J.H., Jeung, I.S., 2013. Effects of a wall on the self-ignition patterns and flame propagation of high-pressure hydrogen release through a tube. *Proc. Combust. Inst.* 34, 2049–2056. https://doi.org/10.1016/j.proci.2012.09.001.

Kotchourko, A., Baraldi, D., Bénard, P., Eisenreich, N., Jordan, T., Keller, J., Kessler, A., LaChance, J., Molkov, V., Steen, M., Tchouvelev, A., 2014. State of the Art and Research Priorities in Hydrogen Safety. Joint Research Centre of the European Commission (JRC), Honolulu, Hawaii.

Lockwood, F. C., Moneib, H. A., 1980. Fluctuating Temperature Measurements in a Heated Round Free Jet. *Combust. Sci. Technol.* 22, 63-81. https://doi.org/10.1080/00102208008952372

Menter, F.R., 1993. Zonal Two Equation kω Turbulence Models for Aerodynamic Flows. *24th Fluid Dynamics Conference*.

Pitss, W.M., 1991. Effects of global density ratio on the centerline mixing behavior of axisymmetric turbulent jets. *Exp. Fluids* 11, 125-134.

Pontiggia, M., Busini, V., Ronzoni, M., Uguccioni, G., Rota, R., 2014. Effect of large obstacles on high momentum jets dispersion. *Chem. Eng. Trans.* 36, 523–528. https://doi.org/10.1016/j.jhazmat.2009.06.064.

Schefer, R., Groethe, M., Houf, W.G., Evans, G., 2009. Experimental Evaluation of Barrier Walls for Risk Reduction of Unintended Hydrogen Releases, *Int. J. Hydrogen Energ.* 34, 1590-1606. https://doi.org/10.1016/j.ijhydene.2008.11.044

Schefer, R.W., Dibble, R.W., 1986. Mixture fraction measuremetns in a turbulent nonreacting propane jet. AIAA paper, 86-0278.

Shell, 2004. FRED – Fire, Release, Explosion and Dispersion, Shell Global Solutions. http://www.shellglobalsolutions.com/hse/software/fred.html. Last access: 15/07/2020.

Souza, A. O., Luiz, A. M., Neto A. T. P., Araujo A. C. B., Silva H. B., Silva A. K., Alves J. J. N, 2019a. A new correlation for hazardous area classification based on experiments and CFD predictions. *Process Saf. Prog.* 38, 21–26. https://doi.org/10.1002/prs.11974.

Souza, A. O., Luiz, A. M., Neto A. T. P., Araujo A. C. B., Silva H. B., Silva A. K., Alves J. J. N, 2019b. CFD predictions for hazardous area classification. *Chinese J. Chem. Eng.* 27, 21–31. https://doi.org/10.1016/j.cjche.2018.06.002

Sposato, C., Tamanini, F., Rogers, W.J., Sam Mannan, M., 2003. Effects of Plate Impingement on the Flammable Volume of Fuel Jet Releases. *Process Saf. Prog.* 22, 4. https://doi.org/10.1002/prs.680220406

Stewart, J.R., 2019. CFD modelling of underexpanded hydrogen jets exiting rectangular shaped openings. *Inst. Chem. Eng. Symp. Ser.* 2019-May.

Tchouvelev, A.V., Cheng, Z., Agranat, V.M., Zhubrin, S.V., 2007. Effectiveness of small barriers as means to reduce clearance distances. *Int. J. Hydrogen Energy* 32, 1409–1415. https://doi.org/10.1016/j.ijhydene.2006.10.020.

Tolias, I.C., Venetsanos, A.G., Comparison of convective schemes in hydrogen impinging jet cfd simulation, 2015. 6th International conference on hydrogen safety (ICHS2015).

Tolias, I. C., Giannissi, S.G., Venetsanos, A.G., Keenan, J., Shentsov, V., Makarov, D., Coldrick, S., Kotchourko, A., Ren, K., Jedicke, O., Melideo, D., Baraldi, D., Slater, S., Duclos, A., Verbecke, F., Molkov, V., 2019. Best practice guidelines in numerical simulations and CFD benchmarking for hydrogen safety applications. *Int. J. Hydrogen Energy* 44, 9050–9062. https://doi.org/10.1016/j.ijhydene.2018.06.005.

Uggenti, A.C., Carpignano, A., Savoldi, L., Zanino, R., 2017. Perspective and criticalities of CFD modelling for the analysis of oil and gas offshore accident scenarios. *Risk, Reliability and Safety: Innovating Theory and Practice: Proceedings of ESREL 2016.*

Van den Bosch, C.J.H., Weterings, R.A.P.M., Duijim, N.J., Bakkum, E.A., Mercx, W.P.M., Engelhard, W.F.J.M., Van den Berg, A.C., Van den Doormaal, J.C.A.M., van wees, R.M.M., 1997. Methods for the calculation of physical effects “Yellow book”. The hague.

Witlox, H.W.M., Holt, A., 1999. A unified model for jet, heavy and passive dispersion including droplet rainout and re-evaporation. CCPS international conference& workshop on modeling the consequences of accidental releases of hazardous materials.

Xu, B.P., Wen, J.X., Tam, V.H.Y., 2011. The effect of an obstacle plate on the spontaneous ignition in pressurized hydrogen release: A numerical study. *Int. J. Hydrogen Energy* 36, 2637–2644. https://doi.org/10.1016/j.ijhydene.2010.03.143.

Zuliani, C., De Lorenzi, C., Ditali, S., 2016. Application of CFD Simulation to Safety Problems – Challenges and Experience Including a Comparative Analysis of Hot Plume Dispersion from a Ground Flare. *Chem.Eng. Trans.* 53, 79-84. https://doi.org/10.3303/CET1653014